Levenberg-Marquardt Level Set Methods for Inverse Obstacle Problems

Martin Burger*

Abstract

The aim of this paper is to construct Levenberg-Marquardt level set methods for inverse obstacle problems, and to discuss their numerical realization. Based on a recently developed framework for the construction of level set methods, we can define Levenberg-Marquardt level set methods in a general way by varying the function space used for the normal velocity. In the typical case of a PDE-constraint, the iterative method yields an indefinite linear system to be solved in each iteration step, which can be reduced to a positive definite problem for the normal velocity. We discuss the structure of this systems and possibilities for its iterative solution.

Moreover, we investigate the application and numerical discretization of the method for two model problems, a mildly ill-posed source reconstruction problem and a severely ill-posed identification problem from boundary data. The numerical results demonstrate a significant speed-up with respect to standard gradient-based level set methods, in particular if topology changes occur during the level set evolution.

Keywords: Level set method, Shape optimization, Gauss-Newton method, Levenberg-Marquardt method, Shape derivatives.

MSC (2000): 49Q10, 35R30, 53C44, 70H20, 90C55

1 Introduction

Level-set methods (cf. [35]) have received growing attention as flexible algorithms for inverse obstacle problems and shape optimization, due to their ability to handle topological changes and to compute reconstructions with minor a-priori information. The frequently used approach still consists in a gradient-type evolution of the level sets (cf. [2, 11, 27, 29, 34, 31, 32, 37]), which generalizes the classical speed method in shape optimization (cf. [30]). This approach and a generalization to general gradient flows (cf. [8, 12]) are able to succesfully compute reasonable reconstructions even if the initial number of connected components does not coincide with those of the solution. As usual for gradient-type methods, the convergence speed is quite slow for such approaches, in particular if the topological structure of the shape changes during the iteration.

The classical fast alternative to gradient-type methods are Newton-type or Gauss-Newton methods. Inexact Newton methods taking into account second derivatives have been applied recently to problems in image segmentation, (cf. [25, 26]), but not yet to inverse obstacle problems. A Gauss-Newton type level set method for a special class of inverse obstacle

*Department of Mathematics, University of California Los Angeles, 520 Portola Plaza, Los Angeles, CA 90095-1555. e-mail: martin.burger@jku.at. On leave from: Industrial Mathematics Institute, Johannes Kepler Universität Linz.

problems, namely those where the output depends on the indicator function of the shape to be identified, has been proposed already by Santosa [37], but was hardly used afterwards. The aim of this paper is to generalize this approach in order to obtain Levenberg-Marquardt type level set methods for general inverse obstacle problems and in a rather general setting. In order to construct such methods we use a framework developed by the author and applied to the construction of general gradient-type methods in [12]. The main idea of this approach is to use a Hilbert space norm for the normal velocity in the shape evolution, which we interpret as the update to be computed by the optimization algorithm. The Levenberg-Marquardt level set method consists in minimizing a quadratic functional in each time step to obtain this normal velocity, and succesively performing a time step for the level set method. The quadratic functionals to be minimized in each time step consist of a Gauss-Newton type approximation to the least-squares functional augmented by a penalty incorporating the squared norm of the normal velocity. Under general assumptions, we verify the well-definedness of this method and show that it has a descent property if the step size is sufficiently small.

As usual for Newton-type methods we expect a significant decrease in the number of iterations compared gradient-type methods, which is confirmed strongly by our numerical experiments. On the other hand the Levenberg-Marquardt method requires the solution of (large) linear systems in each iteration step. Therefore, a significant reduction of numerical effort can be achieved only if these linear systems can be solved in an efficient way. For this reason, we discuss the iterative solution of these linear optimality systems in some detail for two model problems, where the obstacle is related to the output by the solution of partial differential equations with interfaces. We propose to solve an all-at-once formulation of the optimality system (obtained by treating the linearized partial differential equation as a constraint) by preconditioned Krylov subspace methods. We test and compare the behaviour of several block-preconditioners in numerical examples.

The setup of our investigation is as follows: Let $\mathcal{K}_{ad} \subset \mathcal{K}(D)$ be a class of admissible compact sets in $\mathbb{R}^d$, and let $\mathcal{F} : \mathcal{K}_{ad} \to \mathcal{Z}$ be a Frechet-differentiable operator mapping to some Hilbert space $\mathcal{Z}$. Our aim is to solve the nonlinear equation

$$\mathcal{F}(\Omega) = z, \qquad \Omega \in \mathcal{K}_{ad} \tag{1.1}$$

respectively the associated least-squares problem

$$J(\Omega) = \frac{1}{2}\|\mathcal{F}(\Omega) - z\|^2 \to \min_{\Omega \in \mathcal{K}_{ad}} . \tag{1.2}$$

For the representation of the obstacles we introduce a level set function $\phi : \mathbb{R}^d \times \mathbb{R}^+ \to \mathbb{R}$ and define an evolution of shapes by

$$\Omega(t) = \{\ x \in \mathbb{R}^d \mid \phi(x,t) < 0\ \}. \tag{1.3}$$

The evolution of the shapes is obtained by a geometric motion with normal velocity V_n, which is obtained by computing a viscosity solution of the Hamilton-Jacobi type equation

$$\frac{\partial \phi}{\partial t} + \hat{V}_n\ |\nabla \phi| = 0, \tag{1.4}$$

the so-called *level set equation* (cf. [33]). In our subsequent analysis we shall use the level set method as a device to evolve shapes, we shall not discuss the theoretical and numerical details involved with the solution of (1.4) (cf. [33] and the references therein.

The remainder of this papers is organized as follows: In the remaining part we formulate two model problems for inverse obstacle problems, to which we shall apply the Levenberg-Marquardt level set methods. In Section 2, we introduce the Levenberg-Marquardt level set method and analyze some of its basic properties. In the Sections 3 and 4, we discuss the application of the method in detail for the two model problems and give results of several numerical experiments.

1.1 Model Problems

In this section we formulate two model problems for shape reconstruction, a source reconstruction problem from distributed measurements and the identification of cavities from boundary measurements. These problems differ with respect to the problem size and with respect to the kind of ill-posedness. While the first one is "mildly" ill-posed (i.e., the singular values of the linearized shape-to-output map decay with polynomial order), the second problem is known to be "severely" ill-posed (i.e., the singular values decay with exponential order, cf. [3, 17]).

Our first model problem is one of the most simple PDE-constrained inverse obstacle problems, namely the identification of the shape Ω, given the solution u of the elliptic equation

$$-\Delta u = \chi_\Omega, \tag{1.5}$$

subject to homogeneous Dirichlet boundary conditions on ∂D. The weak formulation of this problem reads as follows: find $u \in H_0^1(\Omega) := \{\ u \in H^1(D) \mid u|_{\partial D} = 0\ \}$ such that

$$\int_D \nabla u.\nabla v\ dx = \int_\Omega v\ dx, \qquad \forall\ v \in H_0^1(D). \tag{1.6}$$

Problems of this type (i.e., problems with the domain appearing in the PDE-constraint only via their indicator function) have been considered in the majority of papers on level set methods for inverse problems and the model problem (cf. [24]) represents a canonical example for this class.

The second important type of model problems are those with the boundary Γ appearing in the state equation via a boundary or interface condition. Here we consider the identification of cavities (cf. [3]), which can be formulated as the identification of $\Gamma = \partial\Omega$ from a measurement of the boundary values $u_j \in L^2(\partial D_n)$, $j = 1, \ldots, M$, with the states u_j defined by the boundary value problem

$$\begin{aligned}
\mathrm{div} A\nabla u_j &= 0 && \text{in } D - \Omega, && (1.7)\\
(A\nabla u_j).\nu &= \psi_j && \text{on } \partial D_n && (1.8)\\
u_j &= 0 && \text{on } \partial D_d = \partial D - \partial D_n && (1.9)\\
(A\nabla u_j).\nu &= 0 && \text{on } \Gamma. && (1.10)
\end{aligned}$$

The conductivity matrix A is assumed to be positive definite. This problem has a weak formulation in the space $H_{0,d}^1(\Omega) := \{\ u \in H^1(\Omega) \mid u|_{\partial D_d} = 0\ \}$, which consists in finding $(u_j) \in H_{0,d}^1(\Omega)^M$ such that

$$\sum_j \int_{D-\Omega} (A\nabla u_j).\nabla v_j\ dx = \int_{\partial D_n} \psi_j\ v_j\ dx, \qquad \forall\ (v_j) \in H_{0,d}^1(\Omega)^M. \tag{1.11}$$

This model problem incorporates several typical features of inverse obstacle problems, namely boundary measurements, multiple loads in the state equation, and a boundary condition on the obstacle boundary. A consequence of the latter is that the function space for the state must depend on the obstacle and will thus change during the identification process.

2 Levenberg-Marquardt Level Set Methods

In the following we derive Levenberg-Marquardt methods for inverse obstacle problems using a framework developed by the author in [12] for gradient-type methods using a notion of geometric gradient flows from [4].

2.1 Operator Equations

The general setup for a Levenberg-Marquardt method is to linearize in each step the operator $\mathcal{F}$ in (1.2) and to add a penalty on the update. In the context of the level set method, we can interpret the normal velocity V_n as the update, which is then used to perform a step of the level set equation in a small time interval. With this interpretation, corresponding to the approach in [12], the Levenberg-Marquardt approach can be realized by solving the quadratic problem

$$\frac{1}{2}\|\mathcal{F}(\Omega) + \mathcal{F}'(\Omega)V_n - z\|^2 + \frac{\beta}{2}\|V_n\|_{\mathcal{H}}^2 \to \min_{V_n \in \mathcal{H}}, \tag{2.1}$$

in each step of the iteration, with $F'(\Omega)$ denoting the shape derivative (cf. [16, 38]). Here $\mathcal{H}$ is an appropriate Hilbert space, e.g. $L^2(\Gamma)$ or $H^{\pm\frac{1}{2}}(\Gamma)$ (cf. [12] for an overview of typical Hilbert space norms for the velocity). Note that due to the strict convexity of the functional in (2.1) for $\beta > 0$, there exists a unique velocity $V_n \in \mathcal{H}$ minimizing (2.1).

The weak form for the Levenberg-Marquardt update is given by

$$\langle \mathcal{F}(\Omega) + \mathcal{F}'(\Omega)V_n - z, \mathcal{F}'(\Omega)W_n\rangle + \beta\langle V_n, W_n\rangle_{\mathcal{H}} = 0, \qquad \forall\ W_n \in \mathcal{H}, \tag{2.2}$$

which can be interpreted as a linear equation for the velocity V_n.

The iteration procedure can be summarized as follows:

Algorithm 2.1 (Levenberg-Marquardt Level Set (LMLS) Method). Set $t = 0$, choose initial shape and level set function ϕ_0 such that $\Omega(0) = \{\phi_0 < 0\}$.
Until termination criterion is satisfied do

- Compute the shape $\Omega(t) = \{\phi(.,t) < 0\}$ and the corresponding output $\mathcal{F}(\Omega(t))$.
- Compute the velocity V_n by solving (2.1).
- Extend the velocity V_n to obtain $\hat{V}_n$.
- Choose an appropriate time step τ and evolve the level set function ϕ by solving (1.4) in the time interval $(t, t+\tau)$.
- Set $t = t + \tau$.

Obviously, a fundamental requirement for the use of this method is the well-definedness of the Levenberg-Marquardt step, i.e., the well-posedness of the linear problem (2.2):

Theorem 2.2. *Suppose that the shape derivative of $\mathcal{F}$ exists at Ω and that $\mathcal{F}' : \mathcal{H} \to \mathcal{Z}$ is a bounded linear operator. Then there exists a unique solution of the variational problem* (2.2).

Proof. Under the above assumptions on $\mathcal{F}'$, (2.2) is a standard variational problem of the form

$$a(V_n, W_n) = f(W_n), \qquad \forall\ W_n \in \mathcal{H},$$

with a continuous linear form f and the bilinear form

$$a(V_n, W_n) := \langle \mathcal{F}'(\Omega)V_n, \mathcal{F}'(\Omega)W_n \rangle + \beta \langle V_n, W_n \rangle_{\mathcal{H}}.$$

Due to the Lax-Milgram lemma, the well-posedness of (2.2) is then equivalent to the continuity and coercivity of a. The continuity of a follows from the assumptions on $\mathcal{F}'$, and the coercivity from

$$a(V_n, V_n) = \|\mathcal{F}'(\Omega)\|^2 + \beta \|V_n\|^2_{\mathcal{H}} \geq \beta \|V_n\|^2_{\mathcal{H}}.$$

□

If the time steps are bounded away from zero, then the level set evolution defined by this approach cannot fatten, i.e., the zero level set will not develop interior during the evolution. This is due to the fact that the speed function is stationary in each time interval, for which case a non-fattening result has been obtained in [5].

Another important property for a Levenberg-Marquardt type method is the decrease of the least-squares functional if the iteration has not reached a stationary point.

Theorem 2.3. *Suppose that the shape derivative of $\mathcal{F}$ exists at $\Omega(t_0)$. Then, either $\Omega(t_0)$ is a stationary point of* (1.2) *(with respect to shape derivatives) or there exists a time t_* such that the least-squares functional* (1.2) *is decreasing in the time interval $[t_0, t_*)$, i.e.,*

$$J(\Omega(t)) < J(\Omega(t_0)), \qquad \forall t \in (t_0, t_*). \tag{2.3}$$

Proof. The existence of a shape derivative $\mathcal{F}'(\Omega)$ for the operator $\mathcal{F}$ implies that

$$\frac{d}{dt} J(\Omega(t))|_{t=t_0} = \langle \mathcal{F}(\Omega(t_0)) - z, \mathcal{F}'(\Omega(t_0))V_n) \rangle,$$

and from (2.2) with $W_n = V_n$ we conclude that

$$\frac{d}{dt} J(\Omega(t))|_{t=t_0} = -\beta \|V_n\|^2 - \|\mathcal{F}'(\Omega(t_0))V_n\|^2.$$

If $V_n = 0$, then (2.2) implies that

$$J'(\Omega(t_0))W_n = \langle \mathcal{F}(\Omega(t_0)) - z, \mathcal{F}'(\Omega(t_0))W_n \rangle = 0, \qquad \forall\ W_n \in \mathcal{H},$$

and hence, $\Omega(t_0)$ is a stationary point of J. If $V_n \neq 0$, then $\frac{d}{dt} J(\Omega(t))|_{t=t_0} < 0$ and thus, there exists a time interval $[t_0, t_*)$ with (2.3). □

Theorem 2.3 provides important information on the monotonicity of the least-squares functional. For ill-posed problems in presence of noise, the decrease of the least-squares functional does not imply convergence (cf. [18]). In order to obtain a convergent regularization method one has to use a stopping rule in dependence of the noise level. A natural choice for

such a stopping rule is the discrepancy principle, i.e., one stops the iteration for the minimal value of k such that

$$\|\mathcal{F}(\Omega_k) - z^\delta\| \leq \tau\delta, \tag{2.4}$$

where $\tau > 1$ is an appropriate constant, δ is the noise level, and z^δ denotes the noisy data satisfying

$$\|z - z^\delta\| \leq \delta. \tag{2.5}$$

2.2 PDE-Constrained Problems

In the majority of inverse obstacle problems, the operator $\mathcal{F}$ involves the solution of a partial differential equation, whose coefficients or boundary condition depend on the shape Ω. The typical form of these problems is given by $\mathcal{F}(\Omega) = \mathcal{G}(u_\Omega)$, where the *state* u_Ω is the solution of an equation of the form

$$\mathcal{E}(u; \Omega) = 0. \tag{2.6}$$

For the sake of simplicity we restrict our attention to equations that are affinely linear with respect to u and allow a unique solution u_Ω for each $\Omega \in \mathcal{K}_{ad}$. The shape derivative of $\mathcal{F}$ can be computed by the chain rule, i.e., $\mathcal{F}'(\Omega)V_n = \mathcal{G}'(u_\Omega)u'$, where u' is the solution of

$$\mathcal{E}_0(u'; \Omega) + \mathcal{E}'(u_\Omega; \Omega)V_n = 0, \tag{2.7}$$

where $\mathcal{E}'$ denotes the shape derivative of $\mathcal{E}$ for fixed state u_Ω and $\mathcal{E}_0(., \Omega) := \mathcal{E}(., \Omega) - \mathcal{E}(0, \Omega)$. Note that because of the above assumptions on $\mathcal{E}$, the solution u' of (2.7) exists and is unique.

If we use the weak form of the Levenberg-Marquardt update and the above notation, then we can formulate (2.2) as

$$\langle \mathcal{G}(u_\Omega) + \mathcal{G}'(u_\Omega)u' - z, \mathcal{G}'(u_\Omega)w' \rangle + \beta \langle V_n, W_n \rangle_{\mathcal{H}} = 0, \tag{2.8}$$

for all $W_n \in \mathcal{H}$, where u' solves (2.7) and w' solves

$$\mathcal{E}_0(w'; \Omega) + \mathcal{E}'(u_\Omega; \Omega)W_n = 0. \tag{2.9}$$

By introducing an adjoint variable λ, solving

$$\langle \mathcal{G}(u_\Omega) + \mathcal{G}'(u_\Omega)u' - z, \mathcal{G}'(u_\Omega)w \rangle + \langle \mathcal{E}_0(w; \Omega), \lambda \rangle = 0, \qquad \forall\ w, \tag{2.10}$$

we obtain an symmetric indefinite system for the velocity V_n, the primal variable u', and the dual variable λ, given by

$$\begin{aligned} \langle \mathcal{G}'(u_\Omega)u', \mathcal{G}'(u_\Omega)w \rangle + \langle \mathcal{E}_0(w; \Omega), \lambda \rangle &= \langle z - \mathcal{G}(u_\Omega), \mathcal{G}'(u_\Omega)w \rangle \\ \beta \langle V_n, W_n \rangle_{\mathcal{H}} + \langle \mathcal{E}'(u_\Omega; \Omega)W_n, \lambda \rangle &= 0 \\ \langle \mathcal{E}_0(u'; \Omega), v \rangle + \langle \mathcal{E}'(u_\Omega; \Omega)V_n, v \rangle &= 0, \end{aligned} \tag{2.11}$$

for all test functions v, w, and W_n.

If we rewrite this problem in operator form, we obtain a linear system of the form

$$\begin{pmatrix} A_1 & 0 & K^* \\ 0 & \beta A_2 & L^* \\ K & L & 0 \end{pmatrix} \begin{pmatrix} u' \\ V_n \\ \lambda \end{pmatrix} = \begin{pmatrix} r \\ 0 \\ 0 \end{pmatrix}, \tag{2.12}$$

which is a standard form for PDE-constrained inverse problems (cf. [13, 14, 20, 21]). Under standard assumptions, this linear system is well-posed and allows a finite element approximation of optimal order (cf. [14]), which we shall investigate for our model problems below.

Under the above assumption on $\mathcal{E}$, the operator K is regular and thus, one can eliminate the first and the last equation to obtain the Schur-complement equation

$$(\beta A_2 + L^*(K^*)^{-1}A_1K^{-1}L)V_n = L^*(K^*)^{-1}r. \tag{2.13}$$

The operator in this equation is positive definite for $\beta > 0$ and thus, the discretized version of this system can be solved by standard iterative methods such as conjugate gradients. Since the evaluation of the operator involves the evaluation of K^{-1} and $(K^*)^{-1}$, the solution of the Schur complement system may be rather expensive. As an alternative one can consider the solution of the whole optimality system (2.12) by an iterative method for indefinite systems such as GMRES. Since such an iteration is efficient only for matrices with structured spectra, suitable preconditioning is needed. We shall discuss this issue in further detail for our model problems in the following sections.

Summing up, we can write the algorithm in the case of PDE-constrained problems as:

Algorithm 2.4 (LMLS-Method with PDE Constraints). Set $t = 0$, choose an initial shape $\Omega(0)$ and a level set function ϕ_0 such that $\Omega(0) = \{\phi_0 < 0\}$.
Until termination criterion is satisfied do

- Compute the shape $\Omega(t) = \{\phi(.,t) < 0\}$, the corresponding state $u(t) = u_{\Omega(t)}$ by solving (2.6) for u and the output $\mathcal{F}(\Omega(t)) = \mathcal{G}(u(t))$.
- Compute the velocity V_n by solving (2.11) for (u', V_n, λ).
- Extend the velocity V_n to obtain $\hat{V}_n$.
- Choose an appropriate time step τ and evolve the level set function ϕ by solving (1.4) in the time interval $(t, t+\tau)$.
- Set $t = t + \tau$.

2.3 Inequality Constraints

In some applications, inequality constraints on the domain Ω have to be enforced, in particular one encounters a relation of the form $\Omega \subset D$ for some given (physical) domain in many inverse obstacle problems. In order to incorporate the constraints into the Levenberg-Marquardt level set method, one can again use its shape derivative. I.e., if an inequality constraint of the form

$$\mathcal{C}(\Omega) \leq 0 \tag{2.14}$$

is enforced, then we have to supplement (2.1) by the constraint

$$\mathcal{C}'(\Omega)V_n \leq 0 \qquad \text{if } \mathcal{C}(\Omega) = 0. \tag{2.15}$$

Determining the velocity V_n then requires the solution of a quadratic problem with linear constraints.

For the geometric restriction $\Omega \subset D$, similar reasoning leads to the local constraint

$$V_n(x)\nu_{\partial\Omega}(x).\nu_{\partial D}(x) \leq 0 \qquad \text{if } x \in \partial D \cap \partial\Omega, \tag{2.16}$$

where $\nu_{\partial\Omega}$ and $\nu_{\partial D}$ denote the outward unit normal to ∂D and $\partial\Omega$, respectively.

3 Application to an Inverse Source Problem

In our first model problem, the weak form of the state equation is given by (1.6), which yields

$$\langle \mathcal{E}(u,\Omega), v\rangle = \int_D \nabla u.\nabla v \; dx - \int_\Omega v \; dx, \qquad \forall \; v \in H_0^1(\Omega), \tag{3.1}$$

corresponding to the notation of Section 2. The shape derivative of the operator $\mathcal{E}$ in weak form is given by

$$\langle \mathcal{E}'(u,\Omega)V_n, v\rangle = -\int_\Gamma v \; V_n \; ds, \qquad \forall \; v \in H_0^1(\Omega), \tag{3.2}$$

and the linear part in u is given by

$$\langle \mathcal{E}_0(u,\Omega), v\rangle = \int_D \nabla u.\nabla v \; dx, \qquad \forall \; v \in H_0^1(\Omega). \tag{3.3}$$

The least-squares functional corresponding to a (noisy) observation $z \in L^2(\Omega)$ is given by

$$J(u, V_n) = \frac{1}{2}\int_\Omega |u - z|^2 \; dx + \frac{\beta}{2}\|V_n\|^2_{\mathcal{H}}, \tag{3.4}$$

which means that $\mathcal{G}$ is the embedding operator from $H_0^1(\Omega)$ to $L^2(\Omega)$ and thus $\mathcal{G}'(u) = \mathcal{G}$. In [12], the choice $\mathcal{H} = H^{-\frac{1}{2}}(\Gamma)$ has been proposed as a suitable norm for this model problem, computationally an equivalent norm can be realized by taking the norm in $L^2(D)$ of an extension $\hat{V}_n$ to D.

According to the derivation in Section 2, the optimality system to be solved in each iteration of Algorithm 2 is given by

$$\begin{aligned} \int_D \left(u' \; w + \nabla w.\nabla \lambda\right) \; dx &= \int_D (z-u) \; w \; dx \\ \beta \int_D \hat{V}_n \; \hat{W}_n \; dx - \int_\Gamma \lambda \; W_n \; ds &= 0 \\ \int_D \nabla u'.\nabla v \; dx - \int_\Gamma v \; V_n \; ds &= 0, \end{aligned} \tag{3.5}$$

for all test functions $v, w \in H_0^1(\Omega)$, $W_n \in H^{-\frac{1}{2}}(\Gamma)$, where the integral over Γ has to be understood in a generalized sense due to $V_n, W_n \in H^{-\frac{1}{2}}(\Gamma)$.

3.1 Approximation of the State Equation

In order to approximate the state equation on a fixed grid independent of the shape $\Omega(t)$ respectively the level set function $\phi(.,t)$, we introduce a smoothed function H_ϵ tending to the Heaviside function as $\epsilon \to 0$. Together with the level set function ϕ, we gain an approximation of the weak form (1.6) as

$$\int_D \nabla u.\nabla v \; dx = \int_D H_\epsilon(-\phi) \; v \; dx, \qquad \forall \; v \in H_0^1(\Omega). \tag{3.6}$$

We discretize equation (3.6) by finite elements on a regular triangular decomposition $D = \bigcup_{T\in\mathcal{T}_h} T$, using the subspace

$$\mathcal{V}_h = \{ \; v \in H_0^1(\Omega) \cap C(\Omega) \mid v|_{\partial\Omega} = 0, v|_T \in \mathcal{P}^1(T) \; \},$$

for u and the test functions v. Here and below $\mathcal{P}^k(T)$ denotes the subspace of polynomials of order less or equal than k on T. In order to evaluate the right-hand side we use a piecewise constant approximation of the level set function ϕ on each triangular element, which yields

$$\int_T H_\epsilon(-\phi)v \; dx = H_\epsilon(-\phi|_T) \int_T v \; dx.$$

Hence, the assembly of the linear system to be solved for a given level set is very cheap: the system matrix is the standard discretization of the Laplace operator, which is independent of ϕ as well as the integrals needed for the right-hand side. Thus, the main computational effort can be realized in a preprocessing step, for a given level set function ϕ, we only have to compute a piecewise constant approximation on $\mathcal{T}_h$ and evaluate the smoothed Heaviside function H_ϵ.

3.2 Approximation of the Optimality System

If we use the approximation (3.6) for the state equation, we can derive the corresponding optimality system using the level set equation (1.4). Since the computation of the shape derivative in the original problem can be interpreted as a time derivative with normal velocity V_n, it is natural to compute a "level set derivative" of (3.6) by computing a time derivative and inserting (1.4). This yields the linearized state equation, given in weak form as

$$\int_D \nabla u'.\nabla v \; dx = -\int_D H'_\epsilon(-\phi)\frac{\partial \phi}{\partial t} \; v \; dx = \int_D H'_\epsilon(-\phi)\hat{V}_n|\nabla\phi| \; v \; dx, \tag{3.7}$$

for all $v \in H_0^1(\Omega)$. Note that due to the coarea formula (cf. [19]), we can rewrite the last integral as

$$\int_D H'_\epsilon(-\phi)\hat{V}_n|\nabla\phi| \; v \; dx = \int_{\mathbb{R}} H'_\epsilon(-\rho) \left(\int_{\{\phi(.,t)=\rho\}} \hat{V}_n \; v \; ds \right) \; d\rho,$$

and since H'_ϵ approximates the Dirac-δ distribution, this derivative approximates the original shape derivative $\int_{\{\phi(.,t)=0\}} V_n \; v \; ds$ as $\epsilon \to 0$.

By analogous reasoning as above, we can also derive the optimality system corresponding to the minimization of (3.4) subject to the linearized equation (3.7), given by

$$\begin{aligned} \int_D \left(u' \; w + \nabla w.\nabla\lambda\right) \; dx &= \int_D (z-u) \; w \; dx \\ \beta \int_D \hat{V}_n \; \hat{W}_n \; dx - \int_D H'_\epsilon(-\phi)\hat{W}_n|\nabla\phi| \; \lambda \; dx &= 0 \\ \int_D \nabla u'.\nabla v \; dx - \int_D H'_\epsilon(-\phi)\hat{V}_n|\nabla\phi| \; v \; dx &= 0, \end{aligned} \tag{3.8}$$

We discretize the system (3.8) by finite elements on a regular triangular decomposition $D = \bigcup_{T\in\mathcal{T}_h} T$. We use the subspace $\mathcal{V}_h$ defined above to discretize the linearized state variable u' and the adjoint variable λ, and the subspace

$$\mathcal{H}_h = \{ \; W \in L^2(\Omega) \mid W|_T \in \mathcal{P}^0(T) \; \},$$

to discretize the extended velocity $\hat{V}_n \in L^2(\Omega)$. In addition, we approximate the functions ϕ and $\psi := |\nabla\phi|$ piecewise constant functions, i.e., elements of $\mathcal{H}_h$. This yields the following

discrete approximation: we look for $(u', \hat{V}_n, \lambda) \in \mathcal{V}_h \times \mathcal{H}_h \times \mathcal{V}_h$ satisfying

$$\begin{aligned} \int_D \left(u_h' \; w + \nabla w . \nabla \lambda_h\right) \; dx &= \int_D (z-u) \; w \; dx \\ \beta \int_D V_h \; W \; dx - - \sum_T H_\epsilon'(-\phi|_T) \; W|_T \; \psi|_T \; \int_T \lambda_h \; dx &= 0 \\ \int_D \nabla u_h' . \nabla v \; dx - \sum_T H_\epsilon'(-\phi|_T) \; V_h|_T \; \psi|_T \; \int_T v \; dx &= 0, \end{aligned} \tag{3.9}$$

for all test functions $(w, W, v) \in \mathcal{V}_h \times \mathcal{H}_h \times \mathcal{V}_h$.

3.3 Structure and Solution of the KKT System

By using standard nodal basis functions in $\mathcal{V}_h$ and basis functions supported on single triangles in $\mathcal{H}_h$, we can rewrite (3.9) equivalently as a linear system for the coefficients with respect to these basis functions. Denoting by $\mathbf{p}$ and $\mathbf{r}$ the coefficients of u_h' and λ_h with respect to the basis of $\mathcal{V}_h$ and by $\mathbf{q}$ the coefficients with respect to the basis of $\mathcal{H}_h$, we obtain the linear system

$$\begin{pmatrix} \mathbf{M} & 0 & \mathbf{K}^T \\ 0 & \beta \mathbf{D} & \mathbf{L}^T \\ \mathbf{K} & \mathbf{L} & 0 \end{pmatrix} \begin{pmatrix} \mathbf{p} \\ \mathbf{q} \\ \mathbf{r} \end{pmatrix} = \begin{pmatrix} \mathbf{f} \\ 0 \\ 0 \end{pmatrix}. \tag{3.10}$$

Here $\mathbf{f}$ is a right-hand side arising from the discretized residual $z - u$, and the matrices on the left-hand side are defined as follows:

- $\mathbf{K} = \mathbf{K}^T$ is the standard system matrix corresponding to the discretization of the Laplace operator
- $\mathbf{M}$ is the mass matrix arising from the L^2-scalar products of basis elements in $\mathcal{V}_h$
- $\mathbf{D}$ is a diagonal matrix arising from scalar products in $\mathcal{H}_h$
- $\mathbf{L}$ is a possibly singular but sparse matrix, each of whose element is a multiple of a basis function integrated over a single triangle.

The above system (3.10) has a standard form for the optimality system arising in Levenberg-Marquardt-type methods for PDE-constrained inverse problems, the same structure arises in distributed parameter identification (cf. [14]).

Note that, since we use a fixed triangulation during the level set evolution, most effort needed for assembling the matrices can be carried out in a preprocessing step. The matrices $\mathbf{K}$, $\mathbf{M}$, and $\mathbf{D}$ do not depend on the level set function ϕ at all, the matrix $\mathbf{L}$ can be written as $\mathbf{L} = \mathbf{L}_0\mathbf{C}$, where $\mathbf{L}_0$ is a sparse matrix (of the same size as $\mathbf{L}$) containing all integrals of test functions over single triangles (independent of the level set function), and $\mathbf{C}$ is a diagonal matrix, whose diagonal entries are given by $H_\epsilon'(-\phi|_T) \; \psi|_T$ for each $T \in \mathcal{T}_h$. Hence, the system matrix in (3.10) can be computed very efficiently during the progress of the Levenberg-Marquardt method.

For the numerical solution of the linearized optimality system, we apply the preconditioned GMRES algorithm (cf. [36]). As for all iterative methods, in particular for indefinite systems, the use of an appropriate preconditioning strategy is fundamental for its efficiency.

In order to gain further insight into the structure of the system matrix, we can consider the associated Schur complements, i.e., the system matrix of the linear equation arising when two of the three variables are eliminated. The first one, usually considered for many indefinite systems like the Stokes problem, is obtained by eliminating the primal variables $(\mathbf{p}, \mathbf{q})$ as

$$\mathbf{S}_1 = \mathbf{K}\mathbf{M}^{-1}\mathbf{K}^T + \frac{1}{\beta}\mathbf{L}\mathbf{D}^{-1}\mathbf{L}^T. \tag{3.11}$$

Essentially, the Schur complement $\mathbf{S}_1$ is the sum of a discretized biharmonic operator and a second operator, whose eigenvalues are of order $\frac{1}{\beta}$ on the orthogonal complement of its nullspace. Hence, for small β the spectrum of this matrix may be rather complicated, one may expect that the eigenspace is mainly a decomposition into a subspace close to eigenvectors of the larger eigenvalues $\mathbf{L}\mathbf{D}^{-1}\mathbf{L}^T$ and a second one related to eigenvectors of the biharmonic operator.

The second one is the natural Schur-complement for PDE-constrained optimization, arising from the elimination of the state variable $\mathbf{p}$ and the dual variable $\mathbf{r}$, i.e.,

$$\mathbf{S}_2 = \mathbf{L}^T\mathbf{K}^{-T}\mathbf{M}\mathbf{K}^{-1}\mathbf{L} + \beta\mathbf{D}. \tag{3.12}$$

The Schur complement $\mathbf{S}_2$ is the sum of a discretized compact operator and a regular diagonal matrix multiplied by β. Again, the spectrum may be rather complicated for small β, with a subspace of eigenvectors related to those for large eigenvalues of the first term and a second subspace with eigenvalues of order β.

We investigate the solution of the optimality system using three different preconditioners, namely an indefinite block-preconditioner proposed by Battermann and Sachs [6, 7]

$$\mathbf{P_1} = \begin{pmatrix} 0 & 0 & \hat{\mathbf{K}}^T \\ 0 & \hat{\mathbf{S}}_\mathbf{2} & \mathbf{L}^T \\ \hat{\mathbf{K}} & \mathbf{L} & 0 \end{pmatrix}, \tag{3.13}$$

a block Gauss-Seidel preconditioner of the form

$$\mathbf{P_2} = \begin{pmatrix} \mathbf{M} & 0 & \hat{\mathbf{K}}^T \\ 0 & \hat{\mathbf{S}}_\mathbf{2} & 0 \\ \hat{\mathbf{K}} & 0 & 0 \end{pmatrix}, \tag{3.14}$$

and finally, the inexact Uzawa preconditioner

$$\mathbf{P_3} = \begin{pmatrix} \mathbf{M} & 0 & \hat{\mathbf{K}}^T \\ 0 & \beta\mathbf{D} & 0 \\ \hat{\mathbf{K}} & 0 & -\hat{\mathbf{S}}_\mathbf{1} \end{pmatrix}. \tag{3.15}$$

For these preconditioners, $\hat{\mathbf{K}}$ denotes a preconditioner for the stiffness matrix $\mathbf{K}$ and $\hat{\mathbf{S}}_\mathbf{k}$ denotes a preconditioner for the corresponding Schur complement $\mathbf{S}_\mathbf{k}$, $k = 1, 2$.

Within the setup used for numerical experiments in the following section, we performed tests with the preconditioned GMRES-method for two different triangular discretizations, with 177 respectively 665 inner grid points and 312 respectively 1248 triangles. The total number of unknowns is thus given by 666 on the first and 2578 on the second grid. The regularization parameter is chosen as $\beta = 10^{-7}$.

Preconditioner	GMRES-It.Grid 1	GMRES-It. Grid 2
I	379	1404
$P_1 - I - K$	64	222
$P_1 - J - K$	60	180
$P_1 - J - J$	88	194
$P_2 - S_2 - K$	6	12
$P_2 - I - K$	123	425
$P_2 - J - K$	119	353
$P_3 - S_1 - K$	2	2
$P_3 - J - K$	208	734

Table 1: GMRES-iterations for the optimality systems.

The resulting number of iterations needed to achieve an accuracy of 10^{-6} for different preconditioning strategies are shown in Table 1. The general notation is $P_k - \hat{S}_k - \hat{K}$, where P_k denotes the preconditioner used for the KKT-matrix (as above), $\hat{S}_k$ denotes the type of preconditioning for the associated Schur-complement and $\hat{K}$ the type of preconditioning for the finite element stiffness matrix K. Here, I means preconditioning with a scalar multiple of the identity matrix, J a Jacobian preconditioner, whereas S_k and K mean the use of the exact Schur-complement and stiffness matrix, respectively. The first row shows the result without any preconditioning, which leads to an unreasonable number of GMRES-iterations, as one may expect. The next three rows present results with the block preconditioner P_1, which results in a not small, but still reasonable number of iterations, which do not change strongly with the different preconditioning strategies for the Schur-complement and even for the stiffness matrices K. Note that the application of the third preconditioner $P_1 - J - J$ only enforces the solution of systems with diagonal matrix and is therefore extremely cheap.

The next three rows show results with the block Gauss-Seidel preconditioner P_2, whose application is of compareable numerical effort as P_1. One observes that the number of iterations is extremely low for exact preconditioning of the Schur-complement (which of course enforces unreasonable numerical effort), but the increase in the number of iterations is much stronger than for P_1 if inexact preconditioning of the Schur-complement is used. The same behavior holds in an even more pronounced way for the Uzawa preconditioner P_3, which yields the lowest iteration number on both grids for exact, but the highest for inexact preconditioning of the Schur complement. In general, the number of iterations clearly further increases for any preconditioners if in addition inexact preconditioning is used for the state equation, so that P_1-J-J seems to be a reasonable choice for this problem. In particular, the numerical effort for a step of the LMLS method compares to the one for few steps of a gradient method, where only an adjoint problem with system matrix K has to be solved. For methods using exact preconditioning of the state equation, the iterative method requires many solves with the stiffness matrix K and its adjoint, each them being of the same effort as two steps of the gradient method.

We finally want to mention that the preconditioning techniques we have investigated for this problem are by far not complete, improvement is possible for the choice of the overall preconditioner as well as for the preconditioning of the Schur-complements and the stiffness matrix, where many other tools are available (cf. e.g. [9, 23, 40]). Moreover, a detailed theoretical investigation and comparison of preconditioning strategies is left to future re-

search. However, even among the rather simple block preconditioners above we were able to find a strategy (P_1-J-J) that leads to acceptable effort in each step of the "outer iteration" by the LMLS method, and together with the lower iteration number obtained the Levenberg-Marquardt method outperforms gradient-type level set methods, as we shall see in the following section.

3.4 Numerical Experiments

In the following we report on some numerical experiments with the Levenberg-Marquardt level set method for the source reconstruction problem. We want to reconstruct an obstacle consisting of two distinct circles (plotted blue in all figures), starting from a simply connected initial shape. Numerical experiments for the same setup yield convergence of the gradient-type approach, but a very high number of time steps in [12].

For the discretization of the level set equation we use a high-order WENO finite difference scheme with Godunov flux and TVD Runge-Kutta discretization in time (cf. [28]), which is of 5th order in space and 4th order in time (with time step determined according to the CFL-condition, cf. [33]). The underlying rectangular grid consists of 32×32 cells. The elliptic state equation and the optimality system have been implemented using the finite element discretization above on a grid of 665 interior points and 1248 triangles (within the MATLAB PDE Toolbox). All numerical experiments presented here and below have been implemented within the software system MATLAB. The optimality system arising in each step was solved using preconditioned GMRES with the preconditioner P_1-J-J introduced above.

In order to test the behavior of the method with respect to noise (and to avoid inverse crimes), we generated artificial data by solving the state equation for given exact shape at a very fine adaptive discretization, adding high frequency noise and interpolation to the subsequently used grid. We applied the Levenberg-Marquardt level set method for several different noise levels, monitoring the residual and L^1-error (i.e., L^1-distance between the indicator functions of the reconstructed and exact shape).

Moreover, we use the following simple line search strategy to achieve a descent: we start with a step size close to the one allowed by the CFL-condition and subsequently decrease the step size if no descent is achieved. The step size is accepted if it is less than the CFL step size divided by ten, in order to unreasonably small step sizes. Such a step size selection yields decaying residuals, but surprisingly does not yield a decrease in the number of iterations in general. In some of our numerical experiments, it even happened that the method without step size needed less iterations. This is due to the fact that an increase in the residual during some iteration step usually yields a strong decrease in the following step, which seems to be a rather general effect in level set methods for inverse problems and has been observed also for gradient-type methods (cf. [8, 12]). A further speed up could be achieved by violating the CFL-condition (cf. [33]) in some of the iterations (as e.g. used by Hintermüller and Ring [26]), but if too many large time steps are made, the shapes tend to be very irregular, and new connected components can appear purely due to numerical oscillations.

Figure 1 shows the evolution of the residual (left, semi-logarithmic) and the L^1-error for different noise level, showing typical behavior for iterative regularization methods. First of all, the residual is only decreasing to the order of the noise levels, and secondly, the error in the reconstruction decreases only to a certain value dependent on the noise, while it stagnates or even increases in later stages of the iteration. One also observes that no further decrease of the residual can be obtained after reaching some minimal value. Nonetheless, stopping the

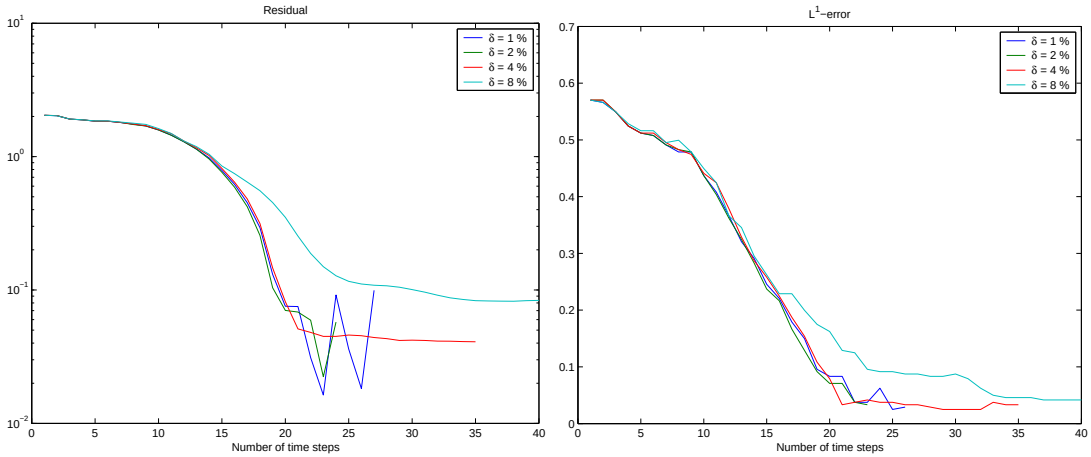

Figure 1: Residual (left) and L^1-error (right) versus number of time steps, for different noise levels.

iteration by the standard discrepancy principle, i.e., using the first index with residual less than $\tau\delta$, yields almost optimal results for typical choices of τ between 1.5 and 2.

The figures 2 and 3 show the evolution of the reconstructed shapes during the LMLS iteration for the noise levels $\delta = 1\%$ and $\delta = 4\%$. One observes that the method is faster for lower noise level and that the final reconstruction is closer for lower noise level, as one would expect. In both cases, the initially simply connected shape splits into three components between iteration 15 and 20, and the smaller third component subsequently vanishes. The quality of the reconstruction is still very good for higher noise level, which is probably caused by the mild ill-posedness of the problem (reconstruction the right-hand side in this elliptic equation is like differentiating twice).

4 Application to the Identification of Cavities

For the identification of cavities, the state equation is given by

$$\langle \mathcal{E}(u,\Omega), v\rangle = \sum_j \int_{D-\Omega} (A\nabla u_j).\nabla v_j \; dx = \int_{\partial D_n} \psi_j \; v_j \; dx, \tag{4.1}$$

and hence, its shape derivative is given by

$$\langle \mathcal{E}'(u,\Omega)V_n, v\rangle = -\sum_j \int_\Gamma V_n \; (A\nabla u_j).\nabla v_j \; dx. \tag{4.2}$$

The linear part in u is simply given by

$$\langle \mathcal{E}_0(u,\Omega)V_n, v\rangle = \sum_j \int_{D-\Omega} \nabla u_j.\nabla v_j \; dx \tag{4.3}$$

The measurements of the traces $u_j \in L^2(\partial D_n)$ induce the least-squares functional

$$\frac{1}{2}\sum_j \int_| u_j' + u_j - z_j|^2 \; dx + \frac{\beta}{2}\|V_n\|^2_{\mathcal{H}}, \tag{4.4}$$

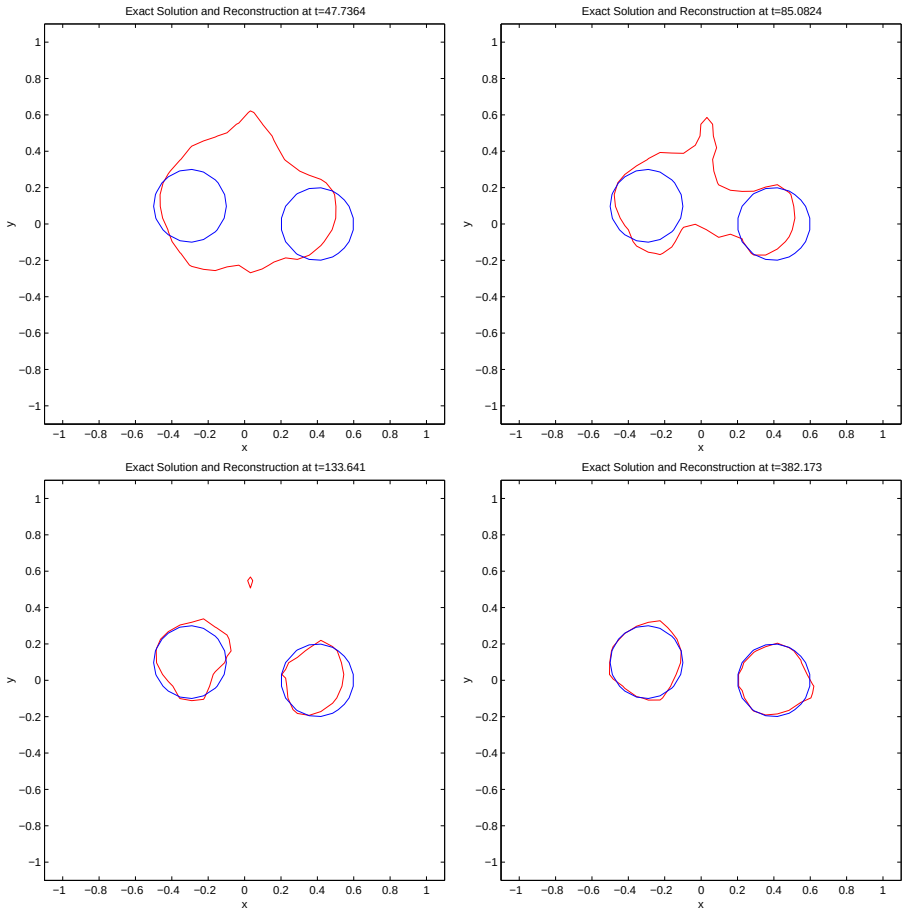

Figure 2: Evolution of the reconstruction (red) and exact shape (blue) for $\delta = 1\%$, $\beta = 10^{-7}$, at time steps 10, 15, 20, 25.

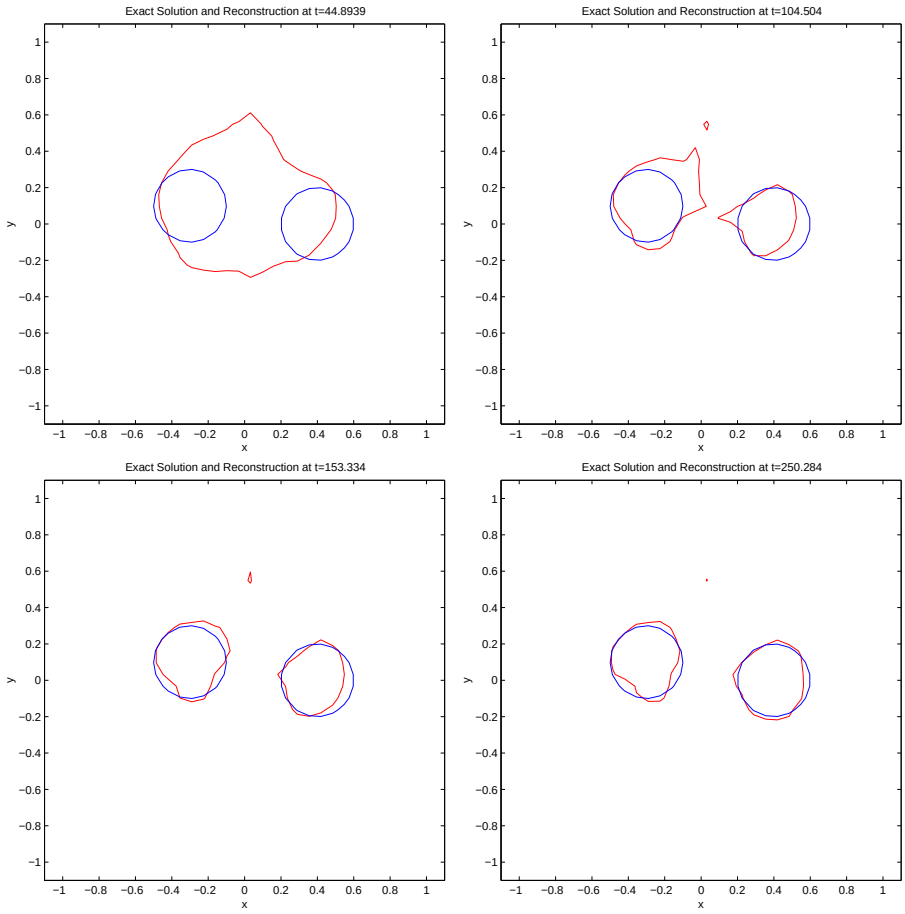

Figure 3: Evolution of the reconstruction (red) and exact shape (blue) for $\delta = 4\%$, $\beta = 10^{-7}$, at time steps 10, 20, 30, 40.

i.e., $\mathcal{G}$ is a direct product of trace operators from $H^1_{0,d}(D-\Omega)$ to $L^2(\partial D_n)$ and due to its linearity $\mathcal{G}'(u)=\mathcal{G}$. In [8, 12], the choice $\mathcal{H}=H^{\frac{1}{2}}(\Gamma)$ turned out to be an appropriate norm for this model problem, which is realized by taking the norm in $H^1(D)$ of an extension $\hat{V}_n$ to D.

As above, we can derive the optimality system to be solved in each iteration of Algorithm 2 is given by

$$\begin{aligned}
\sum_j \int_{\partial D_d} u_j' \; w_j \; ds + \sum_j \int_D (A\nabla w_j).\nabla \lambda_j \; dx &= \sum_j \int_{\partial D_d} (z_j - u_j) \; w_j \; ds \\
\beta \int_D (\nabla \hat{V}_n \; \nabla \hat{W}_n + \hat{V}_n \; \hat{W}_n) \; dx - \sum_j \int_\Gamma W_n \; (A\nabla u_j).\nabla \lambda_j \; ds &= 0 \qquad (4.5) \\
\sum_j \int_D (A\nabla u_j').\nabla v_j \; dx - \sum_j \int_\Gamma V_n \; (A\nabla u_j).\nabla v_j \; ds &= 0,
\end{aligned}$$

for all test functions $v_j, w_j \in H^1_{0,d}(D-\Omega)$, $W_n \in H^{\frac{1}{2}}(\Gamma)$. Note that these KKT equations are system of $2M+1$ partial differential equations for $2M+1$ unknowns.

4.1 Approximation of the State Equation

In order to compute a numerical approximation of the state equation, we use an "ersatz material" approach (cf. [1, 2]), i.e. we use a

$$A_\epsilon = (\epsilon + (1-\epsilon) H_\epsilon(\phi)) \; A, \qquad (4.6)$$

in the whole domain D, where H_ϵ is a smooth approximation of the Heaviside function. Using a straight-forward estimate one can show that the error introduced by this approximation is of order $\sqrt{\epsilon}$ if H_ϵ satisfies standard conditions and if ϕ is sufficiently close to the signed distance function locally around the zero level set Γ.

The arising state equation in weak form is then given by

$$\sum_j \int_D (A_\epsilon \nabla u_j).\nabla v_j \; dx = \int_{\partial D_n} \psi_j \; v_j \; dx, \qquad \forall \; (v_j) \in H^1_{0,d}(D)^M. \qquad (4.7)$$

and can directly by approximated by finite element methods (cf. [10]). In our numerical implementation we choose standard linear finite element methods, i.e., a Galerkin discretization in the subspace

$$\mathcal{V}_h = \{ \; v \in H^1_0(D) \cap C(D) \mid v|_{\partial D_d} = 0, v|_T \in \mathcal{P}^1(T) \; \}.$$

Note that in order to obtain a sufficient resolution of the interface, standard adaptive solution procedures can be used. It seems reasonable to use the grid obtained from an adaptive refinement in the state equation for the solution of the optimality system, too, so that the discretization of the linearized state equation approximates well the linearization of the discretized state equation.

4.2 Approximation of the Optimality System

In an analogous way to the state equation, we can use the ersatz material for the optimality system of the sequential quadratic problems, which then becomes

$$\begin{aligned}
\sum_j \int_{\partial D_d} u_j' \; w_j \; ds + \sum_j \int_D (A_\epsilon \nabla w_j).\nabla \lambda_j \; dx - \sum_j \int_{\partial D_d} (z_j - u_j) \; w_j \; ds &= 0 \\
\beta \int_D (\nabla \hat{V}_n \; \nabla \hat{W}_n + \hat{V}_n \; \hat{W}_n) \; dx + \sum_j \int_D H_\epsilon'(\phi) \; W_n \; (A \nabla u_j).\nabla \lambda_j \; |\nabla \phi| \; ds &= 0 \qquad (4.8) \\
\sum_j \int_D (A_\epsilon \nabla u_j').\nabla v_j \; dx + \sum_j \int_D H_\epsilon'(\phi) \; V_n \; (A \nabla u_j).\nabla v_j \; |\nabla \phi| \; ds &= 0,
\end{aligned}$$

This system can be approximated by standard finite elements, with $u_j', \lambda_j \in \mathcal{V}_h$ and

$$\hat{V}_n \in \mathcal{H}_h = \{ \; v \in H_0^1(D) \cap C(D) \mid v|_{\partial D} = 0, v|_T \in \mathcal{P}^1(T) \; \}.$$

The arising optimality system now has the form (3.10), with different submatrices: $\mathbf{K}$ is a block diagonal matrix consisting of M identical blocks, each representing the stiffness matrix of the differential operator $-\mathrm{div}(A^\epsilon \nabla .)$, and $\mathbf{M}$ is a block diagonal matrix, where each block has nonzero entries only for those indices corresponding to elements adjacent to the measurement boundary. $\mathbf{D}$ is simply the stiffness matrix of the differential operator $-\Delta + I$, and $\mathbf{L}$ is a block matrix with each block representing the discretization of the operator $\hat{V}_n \mapsto -\mathrm{div}(A H_\epsilon'(\phi) \hat{V}_n \nabla u_j)$. The matrices $\mathbf{K}$ and $\mathbf{L}$ depend on the level set function ϕ and change during the iteration.

For the iterative solution of the discretized optimality system we used the GMRES method with two different preconditioning strategies. With the settings of the numerical experiments for the next section , we performed tests at two different fine grids, the first consisting of 1609 nodes and 3096 elements, and the second with 6313 nodes and 12384 elements. The first preconditioning strategy uses again the block preconditioner P_1 of the form (3.13) with different choices for its blocks. The notation is the same as in Section 3, except K_0 denoting a multiple of the stiffness matrix for $-\Delta + I$ as a preconditioner for the Schur complement. The second preconditioning strategy uses the geometric multigrid preconditioner in FEMLAB using two pre-smoothing and one post-smoothing step by the Gauss-Seidel iteration (cf. [39] for multigrid methods). In order to apply smoothers in a reasonable way, we rewrite the optimality system in the form

$$\begin{pmatrix} \mathbf{K}^T & 0 & \mathbf{M} \\ \mathbf{L}^T & \beta \mathbf{D} & 0 \\ 0 & \mathbf{L} & \mathbf{K} \end{pmatrix} \begin{pmatrix} \mathbf{r} \\ \mathbf{q} \\ \mathbf{p} \end{pmatrix} = \begin{pmatrix} \mathbf{f} \\ 0 \\ 0 \end{pmatrix}, \qquad (4.9)$$

i.e., with the highest order differential operators in the diagonal blocks. Note that in this case the smoother (Gauss-Seidel) is the same as the preconditioner P_1 with Gauss-Seidel preconditioners for the stiffness matrix. We test several versions of multigrid preconditioning, denoted by $P_M - k - V\ell$ if V-cycles and $P_M - k - W\ell$ if W-cycles are used. The number k denotes the number of grids used below the first fine grid, i.e., in the case of fine grid 1 we use $k+1$ and in the case of grid 2 we use $k+2$ grid levels for the multigrid preconditioner. On the coarse grid, we obtain a linear system of dimension less than 100×100 that is solved directly

Preconditioner	GMRES-It.Grid 1	GMRES-It. Grid 2
$P_1 - K_0 - K$	16	16
$P_M - 2 - V1$	8	8
$P_M - 2 - W1$	7	6
$P_M - 2 - V2$	5	5
$P_M - 2 - W2$	5	4
$P_M - 1 - V1$	7	7

Table 2: GMRES-iterations for the optimality systems.

by LU-factorization. The value ℓ denotes the number of cycles we run for the multigrid preconditioner.

In table 2 we report the number of GMRES iterations obtained at the first outer iteration in example one, which represents a typical case compared to the results obtained at other outer iterations. We only give the iteration number for the preconditioner P_1 with exact preconditioning of the state equation and a multiple of K_0 as a preconditioner of the Schur-complement, which gave 16 iterations for each grid. Note that an application of this preconditioner is exactly of the same effort as the solution of the state and adjoint equations in a gradient method. Thus, one step of the Levenberg-Marquardt level set method with this preconditioning strategy would correspond to 16 steps of a gradient method, and hence it did yield almost no speed-up of the overall procedure in most of our numerical experiments, since in most cases the gradient method needed around 15 to 25 times the number of steps as the LMLS method. For cheaper versions of P_1 with inexact preconditioning of the state equation as used in the inverse source problem above, the GMRES iteration failed to converge to the desired accuracy of 10^{-6} (with a maximal iteration number of 500 on the first and of 1000 on the second grid). A much better behaviour is found for the multigrid preconditioners introduced above. One observes that for all multigrid tests, the iteration number is below 10, and does not increase for the refined grid (which is due to the case that there is one additional grid level after refinement). The number of iterations needed is compareable to those needed when solving each of the linearized or adjoint state equations with multigrid preconditioning and thus, the numerical effort for solving the linear optimality about the same as in one step of a gradient-type methods. Therefore, one can directly compare the outer iteration numbers between the LMLS and the gradient method in this case, which will clearly show the reduction of numerical effort obtained in the next section.

4.3 Numerical Experiments

For our numerical experiments, we use the same discretization of the level set method as in the first model problem. We chose three different piecewise sinusoidal loads in the state equations, with Dirichlet boundary on the lower segment of the boundary ($y = -1$). The anisotropic conductivity is given by

$$A = \begin{pmatrix} 2 & 0.5 \\ 0.5 & 2 \end{pmatrix}. \tag{4.10}$$

For the discretization of the state equations and the optimality system we used the software package FEMLAB. The regularization parameter is chosen as $\beta = 10^{-4}$ for all computations.

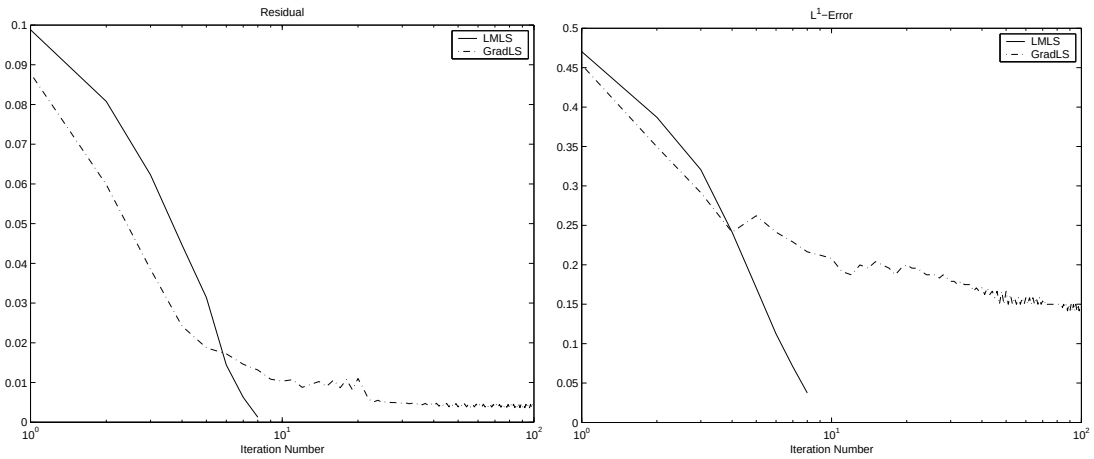

Figure 4: Semi-logarithmic plot of the residual (left) and L^1-error (right) versus number of time steps, for the Levenberg-Marquardt method (solid line) and the gradient-type method (dash-dotted line).

Our first example is the reconstruction of a rather smooth shape, namely an ellipse, with the initial guess being again a circle. The results for almost exact data, i.e., no artificial noise but only numerical errors, are shown in Figures 4 and 5. Figure 4 shows a quantitative comparison of the evolution of residual and L^1-error with the one obtained by the gradient-type level set method. In this case, the Levenberg-Marquardt level set method is able to decrease the residual almost to zero in only nine iteration steps, whereas the gradient-type method needs more than one hundred iterations to decrease the residual to a reasonable size. As usual for these type of methods, the gradient-type approach is slightly faster in the initial stage, but becomes very slow after few iterations. Figure 5 shows the exact and reconstructed shape after 2, 4, 6, and 8 iteration steps. One observes that the shapes approximate the exact solution very well and that convergence is faster in the upper half of the ellipse than in the lower one. This is due to the fact that the upper part is closer to a measurement boundary, whereas there is no measurement in the lower boundary segment $y = -1$ representing the Dirichlet boundary.

Finally, we investigate the behavior with respect to noise by solving the inverse problem for different levels of artificial noise. In order to avoid inverse crimes, we generate the data on a different grid, add Gaussian random noise of relative variance δ and interpolate the data to boundary of the grid used for the solution of the inverse problems. The resulting evolutions of the residual and the L^1-error are shown in Figure 9. One observes that the increase in the L^1-error after obtaining its minimal value is much stronger than for the inverse source problem investigated above, which is due to the stronger instability in the identification of cavitites. The residuals and errors show the expected behavior, one observes that reasonable results for all noise level would be obtained with the discrepancy principle for a choice τ in the interval $[3, 5]$.

In a second numerical test we consider the reconstruction of a shape consisting of two different connected components, a circle and a rectangle. The evolution of the shapes for a noise level $\delta = 0.1\%$ is shown in Figure 7 for the iterates 5, 10, 15, and 20. For this low noise level the shape splits as expected during the level set evolution and one obtains

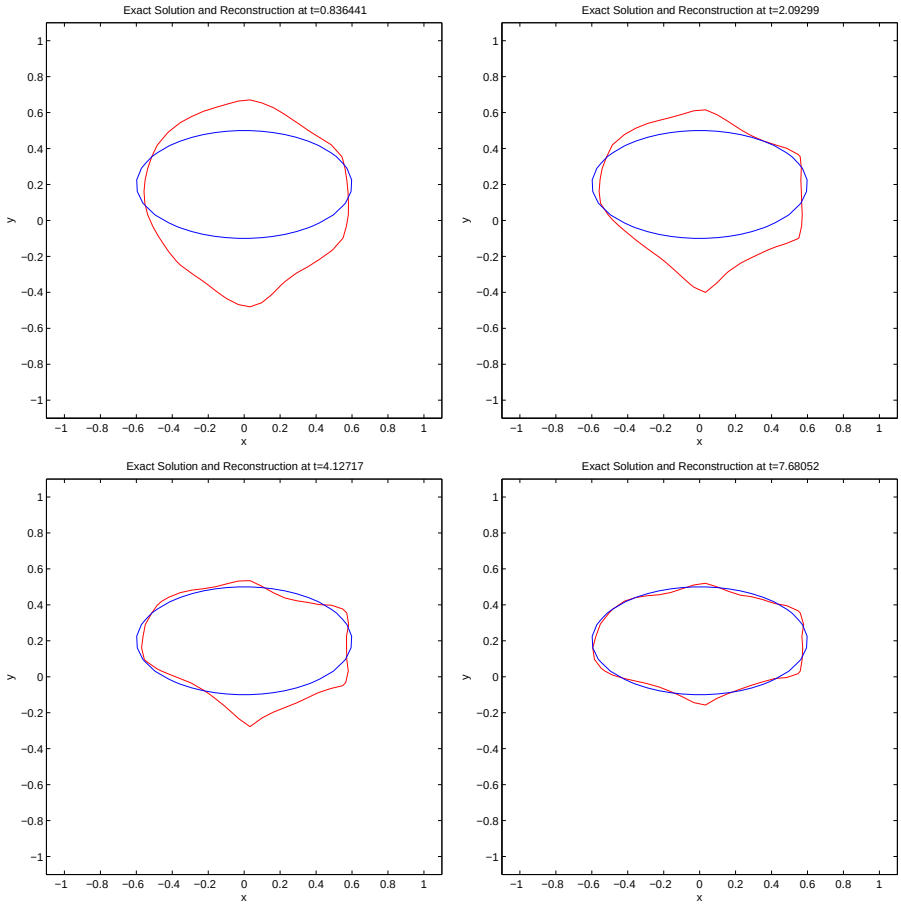

Figure 5: Exact solution (blue) and shapes (red) obtained from the LMLS method at iterates 2, 4 (above), 6, and 8 (below).

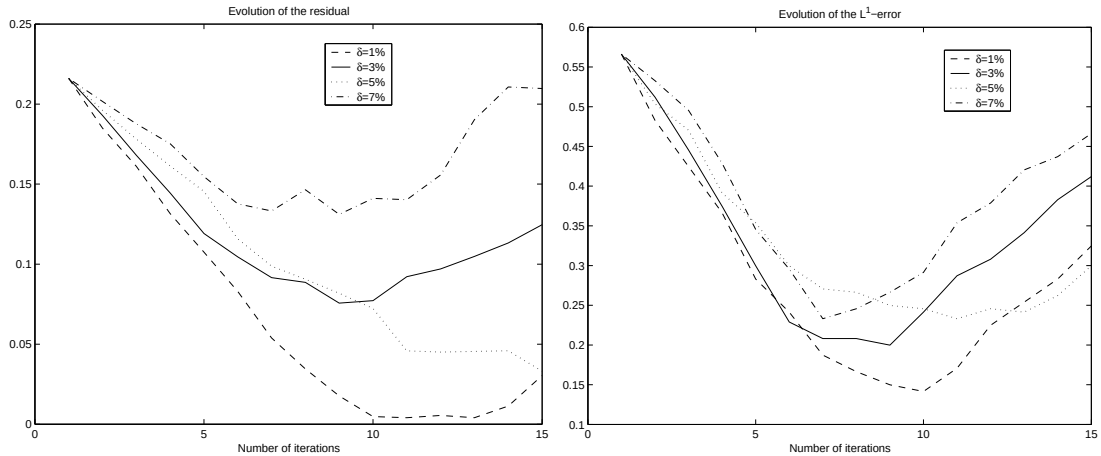

Figure 6: Evolution of the residual (left) and L^1-error in the first example for different noise levels.

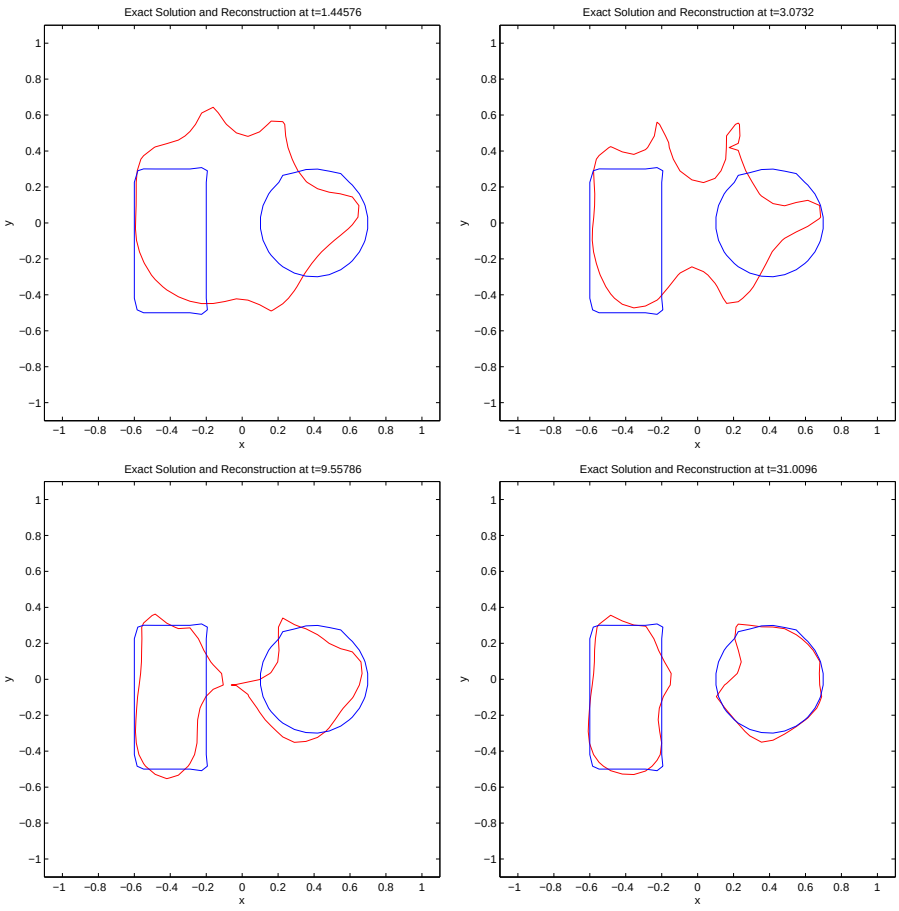

Figure 7: Exact solution (blue) and shapes (red) obtained from the LMLS method at iterates 5, 10 (above), 15, and 20 (below).

a good reconstruction after 20 iteration steps. For higher noise level, the quality of the reconstruction is much lower and splitting does not occur in general. This can be seen from the reconstructions obtained by stopping the LMLS method using the discrepancy principle with $\tau = 4$, plotted in Figure 8.

The evolution of the residual and L^1-error are shown in Figure 9. In this case, one does not obtain reasonable results for large noise levels, in particular we did not observe splitting of the domain during the level set evolution for $\delta > 2\%$. For a noise level of 5% the iteration was not able to compute a better reconstruction than the initial guess. Therefore, we only plot the corresponding curves for noise levels from 1% to 4%. As expected, the number of iterations needed to obtain the best possible reconstruction (or until the method has to be stopped according to the discrepancy principle) increases monotonically with the noise level. Moreover, the total number of iterations for low noise level (also in the noise-free case) is considerably larger as in the first example with a simply connected solution, whereas it is lower for large noise level. The reason for this behavior is the splitting of connected components that occurs for low noise level and slows down the convergence speed.

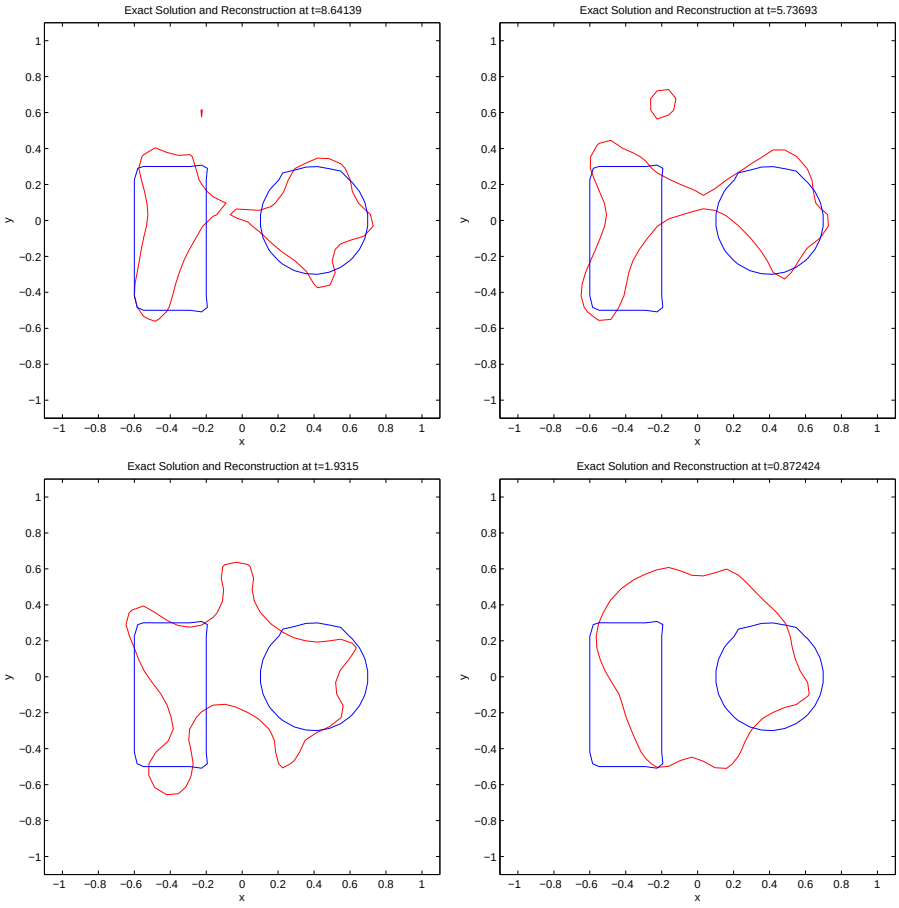

Figure 8: Optimal reconstructions obtained from the LMLS method at noise level $\delta = 1\%$, $\delta = 2\%$ (above), $\delta = 3\%$, and $\delta = 4\%$ (below).

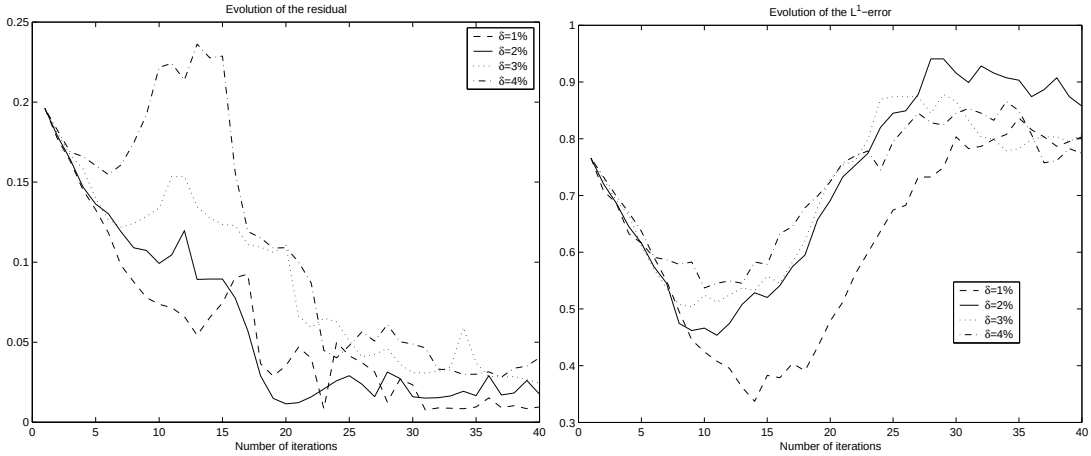

Figure 9: Evolution of the residual (left) and L^1-error (right) in the second example for different noise levels.

Acknowledgments

The author thanks Stanley Osher (UCLA), Fadil Santosa (University Minnesota), Wolfgang Ring (University Graz), Benjamin Hackl, Joachim Schöberl (University Linz), and Wolfram Mühlhuber (Audi AG, Ingolstadt) for useful and stimulating discussions. Financial support is acknowledged by the Austrian Science Foundation FWF under project SFB F 013/08.

References

[1] G.Allaire, *Shape Optimization by the Homogenization Method* (Springer, New York, 2001).

[2] G.Allaire, F.Jouve, A.M.Toader, *A level-set method for shape optimization*, C.R. Acad. Sci. Paris, Ser. I, **334** (2002), 1125-1130.

[3] G.Alessandrini, Luca Rondi, *Optimal stability for the inverse problem of multiple cavities*, J. Diff. Eq. **176** (2001), 356-386.

[4] F.Almgren, J.E.Taylor, *Optimal geometry in equilibrium and growth*, Fractals **3** (1995), 713-723.

[5] G.Barles, H.M.Soner, P.E.Souganidis, *Front propagation and phase field theory*, SIAM J. Control Optim. **31** (1993), 439-469.

[6] A.Battermann, E.W.Sachs, *An indefinite preconditioner for KKT systems arising in optimal control problems*, Technical report (Universität Trier, 2000).

[7] A.Battermann, E.W.Sachs, *Block preconditioners for KKT systems in PDE-governed optimal control problems*, in: R.H.W.Hoppe, K.H.Hoffmann, V.Schulz, eds., *Workshop on Fast Solutions of Discretized Optimization Problems* (Birkhäuser, 2001), 1-18.

[8] H.Benameur, M.Burger, B.Hackl, *Level set methods for geometric inverse problems in linear elasticity*, SFB-Report 2003-12 (SFB F 013, Universität Linz), and submitted.

[9] J.H.Bramble, J.E.Pasciak, P.S.Vassilevski, *Computational scales of Sobolev norms with application to preconditioning*, Math. Comp. **69** (2000), 463-48.

[10] F.Brezzi, M.Fortin, *Mixed and Hybrid Finite Element Methods*, (Springer, New York, 1991).

[11] M.Burger, *A level set method for inverse problems*, Inverse Problems **17** (2001), 1327-1356.

[12] M.Burger, *A framework for the construction of level set methods for shape optimization and reconstruction*, Interfaces and Free Boundaries **5** (2003), 301-329.

[13] M.Burger, W.Mühlhuber, *Iterative regularization of parameter identification problems by SQP-methods*, Inverse Problems **18** (2002), 943-970.

[14] M.Burger, W.Mühlhuber, *Numerical approximation of an SQP-type method for parameter identification problems*, SIAM J. Numer. Anal. **40** (2002), 1775-1797.

[15] T.F.Chan, B.O.Heimsund, T.Kastberg Nilssen, X.C.Tai, *Level set methods and augmented Lagrangian for parameter identification*, Preprint (UCLA, 2002).

[16] M.C.Delfour, J.P.Zolésio, *Shapes and Geometries. Analysis, Differential Calculus, and Optimization* (SIAM, Philadelphia, 2001).

[17] M. DiCristo, L.Rondi, *Examples of exponential instability for elliptic inverse problems* Preprint (2003).

[18] H.W.Engl, M.Hanke, A.Neubauer, *Regularization of Inverse Problems* (Kluwer, Dordrecht, 1996).

[19] L.C.Evans, R.F.Gariepy, *Measure Theory and Fine Properties of Functions* (CRC Press, Boca Raton, 1992).

[20] E.Haber, U.Ascher, *Preconditioned all-at-once methods for large, sparse parameter estimation problems*, Inverse Problems, **17** (2001), 1847-1864.

[21] E.Haber, U.Ascher, D.Oldenburg, *On optimization techniques for solving nonlinear inverse problems*, Inverse Problems **16** (2000), 1263-1280.

[22] M.Hanke, *A regularizing Levenberg-Marquardt scheme, with applications to inverse groundwater filtration problems*, Inverse Problems **13** (1997), 79-95 .

[23] M.Hanke, C.R.Vogel, *Two-level preconditioners for regularized inverse problems I: Theory*, Numer. Math. **83** (1999), 385-402.

[24] F.Hettlich, B.Rundell, *Iterative methods for the reconstruction of an inverse potential problem*, Inverse Problems **12** (1996), 251-266.

[25] M.Hintermüller, W.Ring, *A second order shape optimization approach for image segmentation*, SIAM J. Appl. Math. (2003), to appear.

[26] M.Hintermüller, W.Ring, *An inexact Newton-CG-type active contour approach for the minimization of the Mumford-Shah functional*, J. Math. Imag. Vision (2003), to appear.

[27] K.Ito, K.Kunisch, Z.Li, *Level-set function approach to an inverse interface problem*, Inverse Problems 17 (2001), 1225-1242.

[28] G.S.Jiang, D.Peng, *Weighted ENO-schemes for Hamilton-Jacobi equations*, SIAM J. Sci. Comput. **21** (2000), 2126-2143.

[29] A.Litman, D.Lesselier, F.Santosa, *Reconstruction of a two-dimensional binary obstacle by controlled evolution of a level-set*, Inverse Problems **14** (1998), 685-706.

[30] B.Mohamadi, O.Pironneau, *Applied shape optimization for fluids* (Clarendon Press, Oxford, 2001).

[31] C.Ramananjaona, M.Lambert, D.Lesselier, *Shape inversion from TM and TE real data by controlled evolution of level sets*, Inverse Problems **17** (2001), 1585-1595.

[32] C.Ramananjaona, M.Lambert, D.Lesselier, J.P.Zolesio, *Shape reconstruction of buried obstacles by controlled evolution of a level set: from a min-max formulation to numerical experimentation*, Inverse Problems **17** (2001), 1087-1112.

[33] S.Osher, R.P.Fedkiw *Level Set Methods and Dynamic Implicit Surfaces* (Springer, New York, 2002).

[34] S.Osher, F.Santosa, *Level set methods for optimization problems involving geometry and constraints I. Frequencies of a two-density inhomogeneous drum*, J. Comp. Phys. **171** (2001), 272-288.

[35] S.Osher, J.A.Sethian, *Fronts propagating with curvature-dependent speed: algorithms based on Hamilton–Jacobi formulations*, J. Comp. Phys., **79** (1988), 12-49.

[36] Y.Saad, *Iterative methods for sparse linear systems* (PWS, Amsterdam, 1996).

[37] F.Santosa, *A level-set approach for inverse problems involving obstacles*, ESAIM: Control, Optimisation and Calculus of Variations **1** (1996), 17-33.

[38] J.Sokolowski, J.P.Zolesio, *Introduction to Shape Optimization* (Springer, Berlin, Heidelberg, New York, 1992).

[39] U. Trottenberg, C.W.Oosterlee, A.Schl̈ler, *Multigrid* (Academic Press, London, 2001).

[40] C.R. Vogel and M. Hanke, "Two-level preconditioners for regularized inverse problems II: Implementation and numerical results", Preprint, 1999.